2011 International Nuclear Atlantic Conference - INAC 2011
Belo Horizonte,MG, Brazil, October 24-28, 2011
ASSOCIAÇÃO BRASILEIRA DE ENERGIA NUCLEAR - ABEN
ISBN: 978-85-99141-04-5

NSECT IMAGES ENHANCEMENT USING A LINEAR FILTER IN THE FREQUENCY DOMAIN

Rodrigo S. S. Viana[1], Tiago C. Tardelli[2], Hélio Yoriyaz[3] and Marcel P. Jackowski[4]
[1,2,3]Instituto de Pesquisas Energéticas e Nucleares (IPEN / CNEN - SP)
Av. Professor Lineu Prestes 2242
05508-000 São Paulo, SP, Brazil
[1]rodrigossviana@gmail.com
[2]tiago.tardelli@gmail.com
[3]hyoriyaz@ipen.br

[4]University of São Paulo, Department of Computer Science,
Rua do Matão 1010, São Paulo, SP, Brazil
mjack@ime.usp.br

ABSTRACT

In recent years, a new technique for *in vivo* spectrographic imaging of stable isotopes was presented as Neutron Stimulated Emission Computed Tomography (NSECT). In this technique, a fast neutrons beam stimulates stable nuclei in a sample, which emit characteristic gamma radiation. The photon energy is unique and is used to identify the emitting nuclei. The emitted gamma energy spectra can be used for reconstruction of the target tissue image and for determination of the tissue elemental composition. Due to the stochastic nature of photon emission process by irradiated tissue, one of the most suitable algorithms for tomographic reconstruction is the Expectation-Maximization (E-M) algorithm, once on its formulation are considered simultaneously the probabilities of photons emission and detection. However, a disadvantage of this algorithm is the introduction of noise in the reconstructed image as the number of iterations increases. This increase can be caused either by features of the algorithm itself or by the low sampling rate of projections used for tomographic reconstruction. In this work, a linear filter in the frequency domain was used in order to improve the quality of the reconstructed images.

INTRODUCTION

There are several diseases that are characterized by changes in stable isotopes concentration, and the quantification of these elements, which begin to change even before morphological changes occur in the affected tissues, can provide early in vivo diagnosis of the pathologies. As examples we can cite cases like the difference in concentration of certain chemical elements between benign and malignant tissues [1], quantitative analysis of iron overload in the liver [2], efficiency of nutrients transport [3], changes in concentration of certain elements for Alzheimer's disease [4], kidney disease [5] and heart disease [6].

The stimulated emission tomography by fast neutrons provides a noninvasive alternative to histological analysis with similar results without the need for a surgical procedure. In this technique, a beam of fast neutrons with a low dose rate is used to stimulate stable isotopes of elements in the irradiated media, causing the emission of gamma rays whose energies are characteristic of emitting nuclei. The isotopic composition is determined by obtaining the emission spectrum of interactions from nuclear inelastic scattering, which is then used for the identification of the emitting isotopes. Considering the use of multiple neutron beam projections, it is possible to perform tomographic reconstruction of a qualitative map of the

ISBN: 978-85-99141-04-5

spatial distribution of the nuclei of stable isotopes that are stimulated to emit characteristic gamma rays.

Due to the stochastic nature of photon emission process by irradiated tissue, one of the most suitable algorithms for tomographic reconstruction is the Expectation-Maximization (E-M) algorithm [7]. According to the algorithm formulation are considered simultaneously the photons emission and detection probabilities and these features make this approach one of the most relevant applications of the E-M algorithm. However, after some iterations, the reconstructed images have a certain level of degradation due to noise caused either by features of the algorithm itself as the low sampling rate of projections used for tomographic reconstruction [8].

In this work, a linear filter in the frequency domain was implemented in order to improve the reconstructed images quality. The steps of the image processing aimed highlighting the main features of the reconstructed objects and the suppression of the inherent noise of the tomographic reconstruction. The next sections are organized as follows: in the section 2 will be presented the main related concepts to the NSECT technique, the developed tomographic system as well the simulations environment and the designed linear filter; in the section 3 will be evaluated the obtained results with the tomographic images enhancement and discussions about the reconstructed images quality and conclusion will be done in section 4.

METHODOLOGY

2.1. NSECT and the tomographic system

NSECT is based on inelastic neutron scattering where a beam of fast neutrons stimulate the stable nuclei in a sample, emitting characteristic gamma radiation. The photon energy is unique and is used to identify the emitting nuclei. The gamma spectrum can be used for tomographic reconstruction and spectroscopy of the elements distribution in the sample acquired through a non-invasive *in vivo* scan [9]. In order to reproduce this tomography technique, a monoenergetic collimated neutron source and gamma detectors were virtually simulated with Monte Carlo method assuming all the physical characteristics of the radiation transport.

The Monte Carlo method (MCM) can be described as a statistical method, which uses a sequence of random numbers to perform a simulation. In terms of radiation transport, the stochastic process can be seen as a family of particles moving randomly in each individual collision as they travel through matter. The average behavior of these particles is described in terms of macroscopic quantities such as flux or particle density. The expected value of these quantities corresponds to the deterministic solution of the Boltzman equation. Specific quantities such as deposited energy or dose are derived from these quantities.

In practical applications of the MCM, the physical process is simulated directly, without solving the mathematical equations representing the system behavior. The only requirement needed is that the physical process can be described by a probability density function, which

ISBN: 978-85-99141-04-5

models the physical process of the observed phenomenon. Thus, the essence of MCM applied to radiation transport is to estimate quantities, observing the behavior of a large number of individual events [10].

The MCNP code is a well-known and widely used Monte Carlo code for neutron, photon, and electron transport simulations [11]. The first MCNP version was released in the mid-1970s for neutron and photon transport, and was enhanced over the years to include generalized sources and tallies, electron physics and coupled electron-photon calculations, macrobody geometry, statistical convergence tests and other features. The present work utilized the last MCNP released version which is the version 5. The MCNP5 particle transport simulation requires an input file (inp), which allows the user to specify all the information about geometry modeling, source specifications, material compositions, and the specific quantities to be estimated.

2.1.1. Tomographic system

The simulated tomographic system is based on a first generation computed tomography (CT) scanner. Using this design, the source is modeled as a 7 MeV neutron pencil beam which is translated across the patient to obtain a set of parallel projection measurements at one angle. While in a conventional x-ray CT the source and detector are aligned in opposite sides, in NSECT scanner the detectors should be located at preferentially at 45° around the neutron beam [9]. This feature should be done to minimize counting from inelastic neutron scattering on detectors and, in a experimental approach, neutron detector damage from scattered neutrons.

In order to improve detection efficiency, eight gamma-ray detectors were modeled as cylinders of 10 cm diameter and 9 cm height and have the natural composition of high-purity germanium (HPGe). The detectors are positioned 45 degrees from each other forming a shape-ring detection system of 80 cm diameter and displaced 60 cm from center of CT field of view (FOV). The source/detection system is then rotated slightly and a set of counts is obtained from the track particle transport in detectors during a translation past the sample. This process is repeated once for each projection angle. The Figure 1 exemplifies the simulated tomographic system.

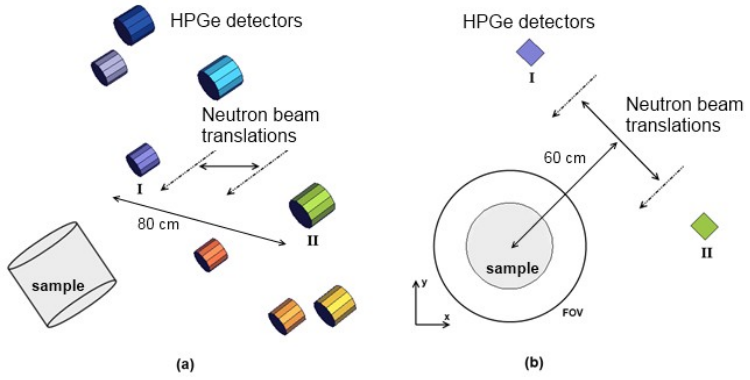

Figure 1. Three-dimensional (a) and two-dimensional (b) perspectives of the simulated tomographic system in a 45 degrees rotation about the y axis.

2011 International Nuclear Atlantic Conference - INAC 2011
Belo Horizonte,MG, Brazil, October 24-28, 2011
Associação Brasileira de Energia Nuclear - ABEN
ISBN: 978-85-99141-04-5

The irradiated sample is a x-ray CT phantom composed by sixteen cylinders of 4 cm diameter and 20 cm height. All of them are symmetrically disposed in a cylinder of 42 cm diameter and 20 cm height made of Lucite. Each one of the sixteen cylinders has a specific composition which simulates some tissues of interest like compact bone, lungs, muscle and fat tissue. More details about these compositions can be found in [12]. The Figure 2 shows this array of cylinders.

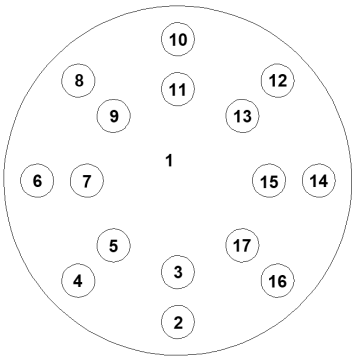

Figure 2. Simulated phantom composed by different materials. Labels are provided in a purpose of matching some regions of interest on tomographic reconstruction.

Each numerical label in Figure 2 refers to a specific chemical composition. According to the Table 1, the materials that composed the phantom are quite different and due to this feature, the tomographic reconstruction of this phantom is a interesting approach for evaluate the potential of NSECT to identify and perform the reconstructions considering the isotopic composition individually.

Table 1. Phantom materials [12].

Label	Phantom material
1	Lucite
2	Spongiosa
3	H + 900
4	Solid water
5	H + 1200
6	RW - 3
7	PMMA
8	H - 800
9	H - 500
10	Compact bone
11	Polyethylene
12	Muscle
13	H + 200
14	Fat
15	H + 400
16	Lung
17	H + 700

2011 International Nuclear Atlantic Conference - INAC 2011
Belo Horizonte,MG, Brazil, October 24-28, 2011
Associação Brasileira de Energia Nuclear - ABEN
ISBN: 978-85-99141-04-5

The simulated sinogram was obtained considering 5975 neutron beam projections where it was performed 239 translations on 25 equidistant angular positions from 0 to 360 degrees. Due to excessive cpu time, it was not possible to simulate the sinogram in high sampling rate, thereby some level of aliasing is expected on reconstructions. The neutron pencil beam was modeled as a square section of 0.25 cm^2 and for each projection were simulated one million neutron histories.

The tomographic reconstructions were performed using E-M algorithm which nowadays is widely employed in emission tomography research. The algorithm features are beyond scope of this paper and more details can be found in [8].

2.2. Unsharp masking in the frequency domain

The reconstructed images using the E-M algorithm usually shows some level of degradation due to ill-posedness of the tomographic reconstruction problem. In addition, depending on the sinogram sampling rate, specific aliasing pattern can be observed in the reconstructed images like streaks. This kind of artefacts can be recognized through high-frequency component of the two dimensional fast Fourier (2D FFT) transform of image under evaluation.

However, some important image features as edges and contrast are also described in the high-frequency component and it is possible that the same image processing can affect in different levels all the high-frequency components. It is desirable to suppress the artefacts as much as possible without compromising any interfaces or contrast levels. Therefore it was implemented the unsharp masking for image enhancement.

According to the literature [13], a low-pass filter g can be used to split an image I into two parts: a smooth part g•I, and the remaining high-frequency part I - g•I containing the edges and other image details. Hence, seems reasonable to describe the image as follow:

$$\mathbf{I} = g \bullet \mathbf{I} + (\mathbf{I} - g \bullet \mathbf{I}), \tag{1}$$

where the expression I − g • I is a approximation of the Laplacian of I. Basically, the unsharp masking enhances the image details by emphasizing the high-frequency component.

Using frequency domain methods, the unsharp masking can be defined according to the equations below:

$$m(x,y) = f(x,y) - f_{LP}(x,y), \tag{2}$$

with

$$f_{LP}(x, y) = = F^{-1}[h_{LP}(u,v) \bullet F(u,v)], \tag{3}$$

where (x,y) and (u,v) are respectively spatial- and frequency- domain variables, $h_{LP}(u,v)$ is a low-pass filter, F(u,v) is the 2D FFT of the input image f(x,y) (pixel value in the spatial

ISBN: 978-85-99141-04-5

domain) and F^{-1} is the inverse discrete Fourier transform (IDFT) [14]. The notation • refers to an array multiplication.

Then, the unsharp masking is composed by the input image f(x,y) and m(x,y) weighted by a penalty parameter:

$$sh(x,y) = f(x,y) - \lambda m(x,y). \quad (4)$$

Using a low-pass gaussian filter, the deviation parameter σ is responsible for the size of the frequency band that is enhanced and λ controls the strength of the enhancement. Small values of σ and λ must highlight the finest details. In this paper it was adopted $\sigma = 5$ for a low-pass gaussian filter in a 200 x 200 reconstructed images size and $\lambda = 0.25$.

RESULTS AND DISCUSSION

According to the basics of the NSECT, it is feasible evaluate individually the isotopes contribution to the gamma spectrum counting and consequently to the tomographic image. In a purpose of demonstrate this feature, the reconstructed image from the full gamma spectrum was compared with partials reconstructions where it was chosen four isotopes of interest.

The most abundant isotope in the phantom materials including compact bones, lungs, muscle and fat tissue is carbon, so it is easy to identify this isotope in the gamma spectrum. The calcium, silicium and magnesium isotopes are located only in a few phantom materials and they are not present in the Lucite chemical composition. The magnesium isotope is present only in the phantom material No. 16, the calcium isotope is found in phantom materials No. 2, 3, 4, 5, 10, 12 13, 15 and 17 and the silicium isotope is found in phantom materials No. 3, 5, 8, 9, 13, 15, 16 and 17.

As previously described, the simulated sinogram considering all the isotopic composition was used first to perform a tomographic reconstruction of irradiated phantom. The Figure 3 shows this initial tomographic reconstruction and its respective 2D FFT. All performed reconstructions were achieved using seven iterations.

2011 International Nuclear Atlantic Conference - INAC 2011
Belo Horizonte,MG, Brazil, October 24-28, 2011
Associação Brasileira de Energia Nuclear - ABEN
ISBN: 978-85-99141-04-5

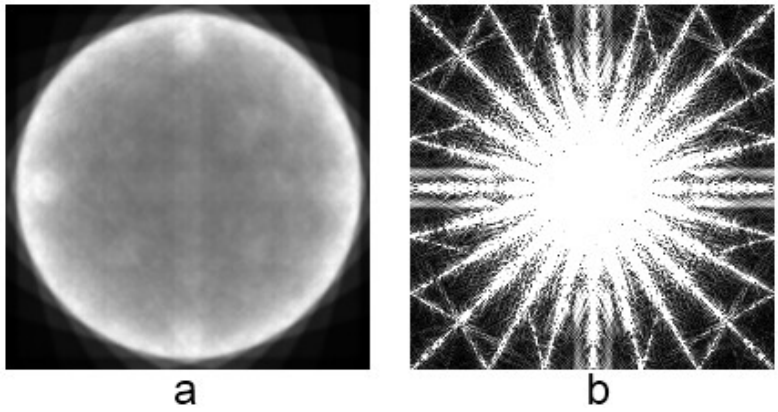

Figure 3. Tomographic reconstruction using the full sinogram (a) and its respective 2D FFT (b).

Due to the low sampling rate of projections, in image appears some artefacts as streaks and this aliasing pattern can be observed through the intense variation in the high-frequency component of the 2D FFT. With respect to the identified phantom materials, apart from Lucite No. 1, only three structures were promptly reconstructed. The reason for that is the low isotopic concentration with regard to carbon abundance.

Using energy windows applied in the original gamma spectra, the counts related to the isotopes under evaluation were used to generate four sinograms and these were input data to perform individual tomographic reconstructions, which reproduces the spatial distribution of each kind of isotope in the irradiated sample. The Figure 4 shows the reconstructions and their respective 2D FFT.

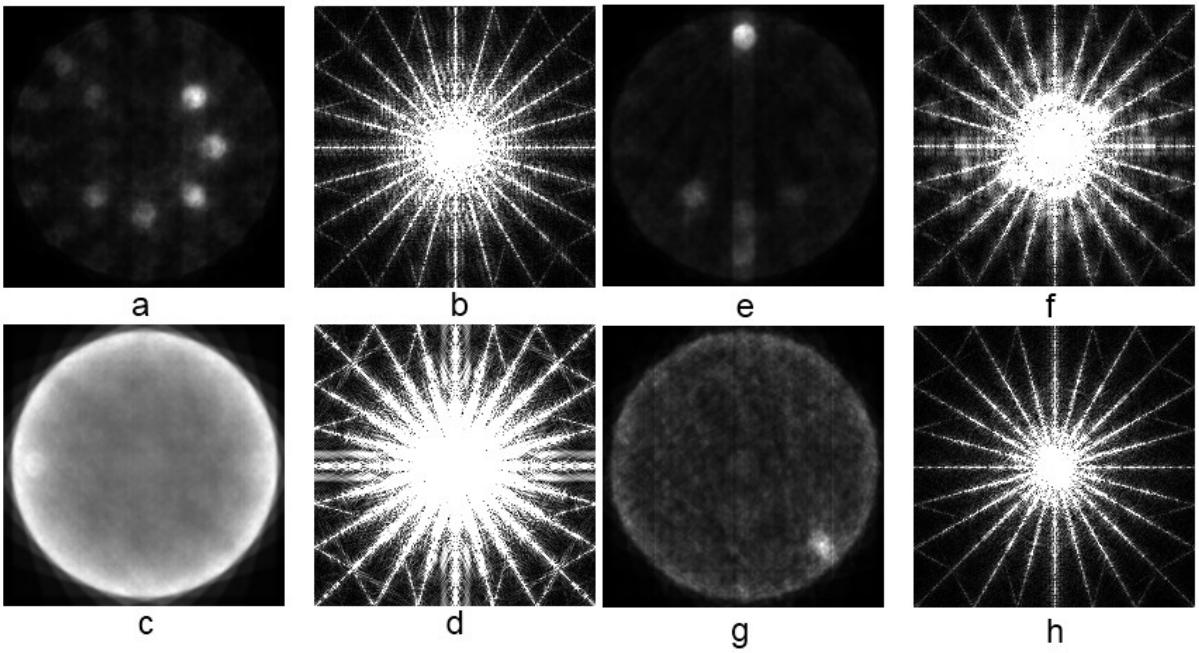

Figure 4. Tomographic reconstructions considering the isolated contribution of distinct isotopes: reconstructions respectively from silicium, carbon, calcium and magnesium isotopes (a, c, e, g) and its respective 2D FFT (b, d, f, h).

2011 International Nuclear Atlantic Conference - INAC 2011
Belo Horizonte,MG, Brazil, October 24-28, 2011
Associação Brasileira de Energia Nuclear - ABEN
ISBN: 978-85-99141-04-5

The Figure 4a shows the magnesium spatial distribution. There are eight phantom materials that contain this isotope and, due to the low concentration, only one phantom material do not appears on the reconstruct image which is No. 16. The carbon spatial distribution is presented on Figure 4c. As expected, this image shows a good definition due to the high carbon concentration. In a particular case, the chemical composition of the phantom material No. 6 shows more than 90 % of carbon. In Figure 4e, the calcium spatial distribution is identified in 5 of the 9 phantom materials where the best identification refers to the compact bone (No. 10) and the magnesium spatial distribution present only in phantom material No. 16 is shown in Figure 4g. Intense streaks appear in the high-frequency component of the 2D FFT due to reconstruction artefacts produced by the low sampling rate of projections.

The neutron pencil beam propagation is not straight forward due to elastic scattering mainly with hydrogen nuclei. Therefore, even setting an energy window on the detected gamma spectra, some undesirable counts appear on sinogram which induces a background in the final reconstructed image. This feature explains the background image on Figures 4a and 4g.

These four partials tomographic reconstructions were processed using the unsharp masking described in previous section. According to the literature, this image processing has the propriety of highlighting the finest details while the image homogeneity is preserved. This image details are very important in order to preserve the reliability between the irradiated sample and reconstructed images. The Figure 5 shows the results of the tomographic images enhancement and their respective 2D FFT.

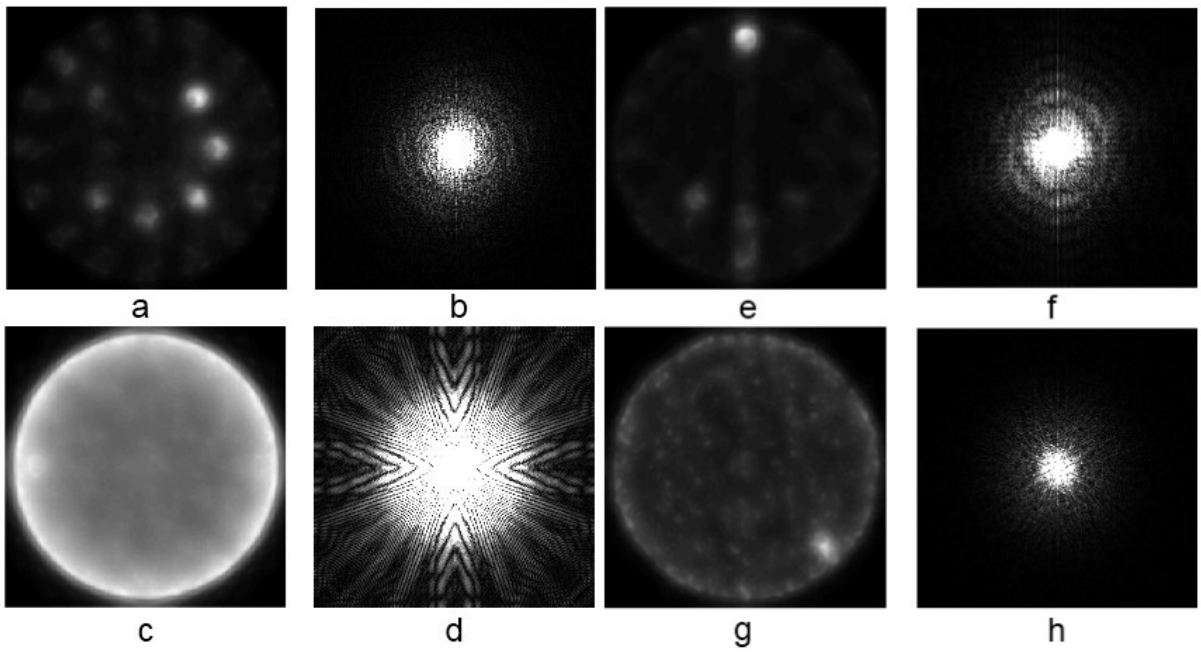

Figure 5. Tomographic images enhancement using the unsharp masking for reconstructions considering the isolated contribution of distinct isotopes: reconstructions respectively from silicium, carbon, calcium and magnesium isotopes (a, c, e, g) and its respective 2D FFT (b, d, f, h).

2011 International Nuclear Atlantic Conference - INAC 2011
Belo Horizonte,MG, Brazil, October 24-28, 2011
Associação Brasileira de Energia Nuclear - ABEN
ISBN: 978-85-99141-04-5

The quality of the images enhancement improved the phantom materials identification presented on Figure 2. Interfaces and contrast levels are in agreement with array of cylinders. The 2D FFT reveals the same pattern of improvement if compared with the Figure 4 as result of the frequencies distribution homogeneity. In all reconstructions, the high-component frequency becomes less intense and this feature suppressed some aliasing artefacts.

Considering the tomographic images enhancement, is expected a quality improvement in an image that contains all of evaluated isotopes. Then, in an additional step, the processed images were fused into a new tomographic image considering simultaneously the four isotopes. The fusion was obtained through the mean pixel value of each reconstructed image which was normalized by the maximum intensity. The Figure 6 shows the fused image.

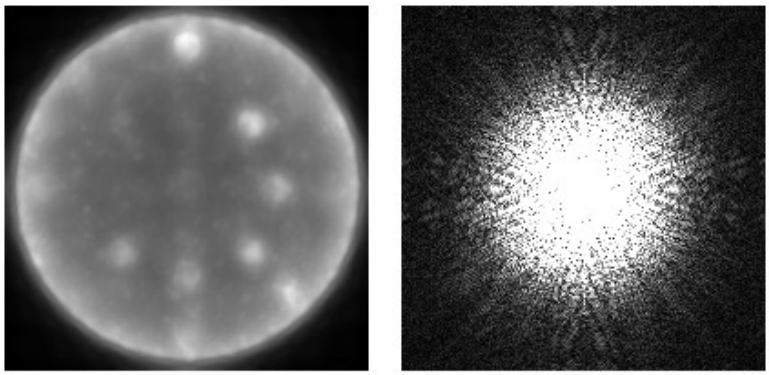

Figure 6. Fusion of the enhanced tomographic images (a) and its respective 2D FFT (b).

Comparing the fused image with the tomographic reconstruction using the original sinogram showed in the Figure 3, it is possible to observe better contrast levels and the identification of phantom materials becomes clearer. Other important details are the preservation of edges in addition of the identification of more phantom materials than first tomographic reconstruction, besides aliasing artefacts were suppressed. The superior quality of the fused tomographic image can be also evaluated through its 2D FFT which shows a homogeneous distribution of the frequencies including the high-frequency component when compared with 2D FFT of the first tomographic reconstruction. In order to compare the reconstruction improvement, the edges of reconstructions showed on Figures 3a and 6a were detected using the Canny method, Figure 7.

2011 International Nuclear Atlantic Conference - INAC 2011
Belo Horizonte,MG, Brazil, October 24-28, 2011
Associação Brasileira de Energia Nuclear - ABEN
ISBN: 978-85-99141-04-5

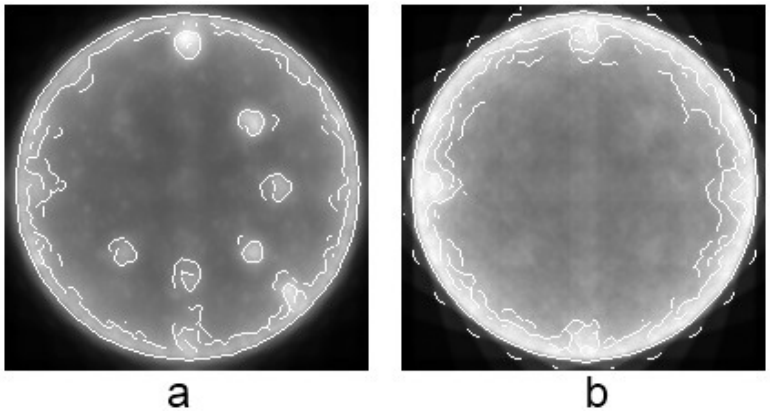

Figure 7. Canny edge detector applied on fused image (a) and tomographic reconstruction from original gamma spectra (b).

According to the edge detection, some unidentified phantom materials initially reconstructed from original gamma spectra becomes visible on fusion of the enhanced tomographic images, specially the inner ones. Another important feature observed through the outer contours is the artefacts suppressing without compromising the phantom-air interface. These improvements on the fused image justify the proposed methodology in an effort to emphasize the main details of each processed image while phantom material identification is preserved.

The simulated phantom is composed by seventeen cylinders made of different materials, but at least one isotope is common among all of them. Therefore, it would be expected that all cylinders were identified in some isotopic individual reconstruction or in the fused image. This statement is correct, however there are some details that should be discussed before concluding whether the NSECT technique can or cannot provide useful information, and especially in what situations.

Basically there are two factors that affect the NSECT performance which are neutron beam and composition related. As mentioned before, the neutron pencil beam propagation is not straight forward due to elastic scattering. Then, even in a collimated configuration, the neutron beam stimulates the surrounding area of beam path. Considering this fact, on each neutron beam projection, the photon emission cannot be originated in a region well-known. This implies in a poor resolution for reconstruction of small structures.

The influence of composition over the reconstruct images is dependent of the similarity among chemical components. The simulated phantom was intentionally proposed in order to demonstrate this feature. The unidentified phantom materials has chemical compositions very similar, and in association with the neutron beam scattering it was not possible to distinguish then due to the small difference of counting between successive neutron beam translations.
Now a days different modalities of diagnosis can provide complementary information about anatomy and physiology. However, there are few of them that can quantify the tissue composition in a noninvasive procedure. Even considering the drawbacks related to resolution and identification of small structures, the NSECT technique is able to provide simultaneously anatomic and physiologic information about a range of pathologies.

ISBN: 978-85-99141-04-5

According to the literature, the breast cancer detection [15], the assessment of calcium deposition related to breast microcalcifications development [16], and evaluation of iron overload in liver [17] are examples of applications where the absorbed dose can be compared with x-ray CT scan or conventional x-ray image.

CONCLUSION

The proposed methodology was able to improve the reconstructed tomographic image in association with the isotopic individual selection. In the present approach, it was demonstrated the capacity of the NSECT technique in perform tomography for isolated isotopes.

Due to additional noise associated to the E-M algorithm and aliasing artefacts from histogram sampling, image processing become necessary in order to improve the reconstructed image quality. According to the obtained results, besides image quality improvement, the image processing revealed details unobserved when the images were fused. Using this approach the fused image from the enhanced images revealed more phantom materials than tomographic reconstruction from original sinogram without any processing technique.

The tomographic image enhancement was achieved by implementation of the unsharp masking in the frequency domain and this filter shows good properties for this application by suppressing artefacts and highlighting finest details without compromising edges or contrast levels.

Initially the NSECT technique was proposed aiming at anatomic images reconstructions, but considering the potential for isotopic identification, it is clear that NSECT can be used for a functional approach, once specific isotopes could be associated with pathologies or some physiological states.

ACKNOWLEDGMENTS

The authors would like to thank the Fundação de Amparo à Pesquisa do Estado de São Paulo – FAPESP by financial suport grant no. 2010/04206-4.

REFERENCES

1. Z. Dobrowolski, T. Drewniak, W. Kwiatek, P. Jakubik, " Trace elements distribution in renal cell carcinoma depending on stage of disease". *Eur. Urol.*, **v.42**, p.475–480 (2002).
2. Kapadia, A. "Accuracy and patient dose in neutron stimulated emission computed tomography for diagnosis of liver iron over- load: simulations in GEANT4". 2007. PhD Thesis, Department of Biomedical Engineering, Duke University, Durham, North Carolina, EUA.
3. J. Stedman, N. Spyrou, " Major and trace element concentration differences between right and left hemispheres of the normal human brain". *Nutrition*, **v.11**, p.542–545 (1995).
4. J. Mutter, J. Naumann, R. Schneider, H. Walach, "Mercury and Alzheimers Disease".

ISBN: 978-85-99141-04-5

Fortschr Neurol. Psychiatr., **v.75**, p. 528-538 (2007).
5. Chmielnicka, J.; Nasiadek, M. "The trace elements in response to lithium intoxication in renal failure". *Ecotoxicol. Environ. Saf.*, **v.55**, p.178-183 (2003).
6. E. Altekin, C. Coker, A. Sisman, B. Onvural, F. Kuralay, O. Kirimli, "The relationship between trace elements and cardiac markers in acute coronary syndromes". *J. Trace Elem. Med. Biol.*, **v.18**, p. 235-242 (2005).
7. A. Dempster, N. Laird, D. Rubin, "Maximum Likelihood from Incomplete Data via the EM Algorithm". *Journal of the Royal Statistical Society Series B*, **v.39**, p. 1-38 (1977).
8. G. Mclachlan, T. Krishnan, *The EM Algorithm and Extensions*. John Wiley and Sons, New York, USA, 1997.
9. C. Floyd Jr, C. Howell, B. Harrawood, A. Crowell, A. Kapadia, R. Macri, J. Xia, R. Pedroni, J. Bowsher, M. Kiser, G. Tourassi, W. Tornow, R. Walter, "Neutron Stimulated Emission Computed Tomography of Stable Isotopes". *Proceedings of SPIE*, Bellingham, **v.5368**, p.248-254 (2004).
10. H. Yoriyaz, "Monte Carlo Method: principles and applications in Medical Physics". *Revista Brasileira de F´ısica Me´dica*, **v.3**, p.141-149 (2009).
11. F. Browm, R. Barrett, T. Booth, J. Bull, L. Cox, R. Forster, T. Goorley, R. Mosteller, S. Post, R. Prael, E. Selcow, A. Sood, J. Sweezy, "MCNP Version 5". Applied Physics Division - Los Alamos National Laboratory, LA-UR-02-3935, 2002.
12. S. Schneider, T. Bortfeld, W. Schlegel, "Correlation between CT numbers and tissue parameters needed for Monte Carlo simulations of clinical dose distributions". *Phys. Med. Biol.*, **v.45**, p.459–478 (2000).
13. Suetens, P. *Fundamentals of Medical Imaging*. Cambridge University Press, New York, USA, 2009.
14. Gonzales, R.; Woods, R. *Digital Imaging Processing*. Prentice Hall, New York, USA, 2001.

15. A. Kapadia, A. Sharma, G. Tourassi, J. Bender, C. Howell, C. Floyd Jr, C. Howell, A. Crowell, M. Kiser, B. Harrawood, R. Pedroni, "Neutron Stimulated Emission Computed Tomography for Diagnosis of Breast Cancer," *IEEE Transactions on Nuclear Science*, **v.55**, pp.501-509 (2008).
16. R. Viana, H. Yoriyaz, "NSECT applied to the assessment of calcium deposition due to the presence of microcalcifications associated with breast cancer". *In Proceedings of the 18 th International Conference on Medical Physics*, Porto Alegre, 2011.
17. A. Kapadia, G. Tourassi, A. Sharma, A. Crowell, M. Kiser, C. Howell, "Experimental detection of iron overload in liver through neutron stimulated emission spectroscopy". *Phys. Med. Biol.*, **v.53**, p.2633-2649 (2008).